INTERNATIONAL JOURNAL FOR NUMERICAL METHODS IN FLUIDS
Int. J. Numer. Meth. Fluids, **26**: 1127–1154 (1998).

FINITE ELEMENT ANALYSIS OF TRANSIENT FLUID FLOW WITH FREE SURFACE USING VOF (VOLUME-OF-FLUID) METHOD AND ADAPTIVE GRID

J. H. JEONG AND D. Y. YANG*

Department of Mechanical Engineering, Korea Advanced Institute of Science and Technology, Taejon, South Korea

SUMMARY

The VOF method is adopted for the finite element analysis of transient fluid flow with a free surface. In particular, an adaptation technique for generating an adaptive grid is incorporated to capture a higher resolution of the free surface configuration. An adaptive grid is created through the refinement and mergence of elements. In this domain the elements in the surface region are made finer than those in the remaining regions for more efficient computation. Also, three techniques based on the VOF method are newly developed to increase the accuracy of the analysis, namely the filling pattern, advection treatment and free surface smoothing techniques. Using the proposed numerical techniques, radial flow with a point source and the collapse of a dam are analysed. The numerical results agree well with the theoretical solutions as well as with the experimental results. Through comparisons with the numerical results of several cases using different grids, the efficiency of the proposed technique is verified. © 1998 by John Wiley & Sons, Ltd.

KEY WORDS: free surface; transient viscous incompressible fluid; finite element method; VOF (volume-of-fluid) method; adaptive grid

1. INTRODUCTION

In order to understand the physical phenomena of general fluid flow, transient fluid flow with a free surface has long been subject to extensive investigations. For the analysis of material manufacturing processes such as casting and polymer processing, the method of such analysis is widely employed. For the numerical analysis of transient fluid flow with a free surface, three approaches have been developed over the years, namely the Lagrangian,[1,2] ALE (arbitrary Lagrangian–Eulerian)[3–5] and Eulerian[6–19] methods.

In the Lagrangian method a moving mesh system is used and the formulation does not include the non-linear convection terms. If a good quality of mesh is maintained, the numerical results of velocity, pressure and predicted position of the free surface are very accurate. When the flow of the fluid is very complex or folding of the flow occurs, remeshing techniques requiring the knowledge

* Correspondence to: D. Y. Yang,Department of Mechanical Engineering, Korea Advanced Institute of Sciece and technology, 373-1, Kusong-dong, Yusong-gu, Taejon 305-701, South Korea. E-mail: dyyang@hanbit.kaist.ac.kr

CCC 0271–2091/98/101127–28 $17.50
© 1998 John Wiley & Sons, Ltd.
Received September 1996
Revised March 1997

and experience of an expert are needed, since the mesh becomes severely distorted. The ALE method combines the merits of the Lagrangian and Eulerian methods to increase the accuracy of the numerical results. However, remeshing is still required for general cases. In the Eulerian method the Eulerian formulation and a fixed mesh system are used. Therefore treatment of the non-linear terms of the governing equations is necessary, but no remeshing procedure for a distorted mesh is needed. The Eulerian method is widely used for the analysis of general and complex problems, since the remeshing procedure is not required. Then the element domain to be computed by the FEM (finite element method) can be composed of the initial mesh[11–14] or a new mesh system[6–10,15–19] regenerated from the initial mesh.

For dividing the fluid and empty regions of the total domain, the MAC (marker-and-cell) method of Harlow and Welch[6] and the VOF (volume-of-fluid) method of Hirt *et al.*[9] have been typically used. In the MAC method the total domain is divided into fluid and empty regions by distinguishing whether a marker exists or not. A marker has no mass and moves according to the velocity field. The position of the free surface and the flow phenomena inside the fluid region are described by the distribution of markers. The MAC method requires sufficient memory size in order for the markers to be distributed in the fluid region.

In the VOF method, fractional volumes are used to divide the total domain. The values of the fractional volumes in the filled, partially filled and empty cells are unity, between zero and unity, and zero respectively. In the VOF method, only one scalar value of the fractional volume is required for each cell and the fractional volume at the current time step in each cell is calculated using the velocity field and fractional volume of the previous time step. The VOF method is a very efficient method for analysing transient fluid flow with a free surface. However, it has drawbacks in that the position of the free surface is predicted only by the scalar fractional volume value and the filling state of its neighbour cells, defined as cells sharing a common side.

In this study, for the finite element analysis of transient fluid flow with a free surface, the VOF method in conjunction with the Eulerian method is used. The element domain is composed of a quadrilateral mesh system and the grid is composed of quadrilateral elements. The element domain is used for FEM analysis, while the grid is used for calculation of the fractional volume and generation of the element domain. The element domain is generated by using selected elements from the grid for efficient computation. In previous studies the grid could not be adaptively altered during the analysis. Therefore the quality of the initial grid was very important for numerical analysis, and, in general, to increase the accuracy of the numerical results, the number of initial elements should be increased. However, increasing the number of elements in the initial grid increases the required computation time and memory size by geometric progression, since the total number of elements in the element domain is increased.

In this paper, in particular, an adaptive grid is incorporated with the FEM and VOF method to capture a higher resolution of the free surface configuration. The element domain is generated and the free surface is predicted by using an adaptive grid where the elements are regenerated efficiently at each time step. The adaptive grid for the current time step is generated by refining and merging the elements in the grid for the previous time step. In an adaptive grid the elements in the surface region are finer than those in other regions. Also in this study, three techniques based on the VOF method are developed to increase the accuracy of the analysis. The first approach is filling pattern technique to predict the free surface by considering the geometric shape of each quadrilateral element. The second approach is the advection treatment technique to calculate the fluid advection iteratively and forcedly. The third approach is the smoothing technique to improve the non-smoothness of the predicted free surface. The Navier–Stokes and continuity equations form the governing equations, and for the FEM formulation the penalty and predictor–corrector methods are used. By using the proposed analysis techniques, radial flow with one point source and the collapse of a dam are analysed and compared

 © 1998 John Wiley & Sons, Ltd.

with theoretical solutions and experimental results. Also, to verify the efficiency of this method, numerical analyses are accomplished for several cases using different grids.

2. GOVERNING EQUATIONS

The governing equations for transient incompressible viscous flow with a free surface are the continuity equation

$$\frac{\partial u_i}{\partial x_i} = 0 \quad \text{in } \Omega \tag{1}$$

and the Navier–Stokes equation

$$\rho \frac{\partial u_i}{\partial t} + \rho u_j \frac{\partial u_i}{\partial x_i} = \frac{\partial}{\partial x_j} \sigma_{ji}(u) + \rho f_i \quad \text{in } \Omega, \tag{2}$$

where

$$\sigma_{ij} = -p\delta_{ij} + 2\mu d_{ij}, \qquad d_{ij} = \frac{1}{2}\left(\frac{\partial u_i}{\partial x_j} + \frac{\partial u_j}{\partial x_i}\right).$$

In the above equations, t, u_i, p, ρ, μ and f_i are the time, velocity component in the x_i-direction, pressure, density, dynamic viscosity and body force respectively and σ_{ij} and d_{ij} denote the stress and strain tensors respectively.

On the free surface boundary $\partial\Omega_{\text{front}}$ the equilibrium condition for stress, i.e.

$$\begin{aligned} \sigma_{\text{n}} &= -p + 2\mu_{\text{air}} \frac{\partial u_{\text{n}}}{\partial x_{\text{n}}} = 0 \quad \text{on } \partial\Omega_{\text{front}}, \\ \tau &= \mu_{\text{air}}\left(\frac{\partial u_{\text{n}}}{\partial x_{\text{t}}} + \frac{\partial u_{\text{t}}}{\partial x_{\text{n}}}\right) = 0, \end{aligned} \tag{3}$$

is imposed, where σ_{n}, τ, μ_{air} and subscripts 'n' and 't' denote the normal stress, shear stress, dynamic viscosity of air and normal and tangential directions of the free surface respectively. On the free surface the surface tension, viscous stress and gas pressure are assumed to be zero in this study. Then the following free-slip condition is applied to the wall boundary $\partial\Omega_{\text{wall}}$,

$$u_{\text{n}}^{\text{w}} = 0 \quad \text{on } \partial\Omega_{\text{wall}}, \tag{4}$$

where u_{n}^{w} is the normal velocity component at the wall boundary, and the following essential boundary condition is applied to the inflow boundary $\partial\Omega_{\text{inflow}}$,

$$u_i = \overline{u_i} \quad \text{on } \partial\Omega_{\text{inflow}}, \tag{5}$$

where $\overline{u_i}$ is the velocity component which is given at the inflow boundary.

The initial conditions are given by specifying the velocity values at the initial time:

$$u_i = u_i^0 \quad \text{on } \Omega \quad \text{at } t = 0, \tag{6}$$

where u_i^0 is the initial velocity component.

© 1998 John Wiley & Sons, Ltd.

3. FINITE ELEMENT FORMULATION

The Navier–Stokes and continuity equations are discretized by using the penalty function formulation and Galerkin formulation[20,21] for the four-node quadrilateral element. In the penalty function formulation of (1) and (2) the constitutive equation is replaced by

$$\sigma_{ij} = \lambda d_{kk}\delta_{ij} + 2\mu d_{ij}, \tag{7}$$

where λ is the penalty constant, taken to be positive and sufficiently large.

In the Galerkin formulation of (2) and (7) the weak form is obtained as

$$\int_\Omega (\rho \dot{u}_i \bar{u}_i + \rho u_j u_{i,j} \bar{u}_i + \lambda u_{j,j} \bar{u}_{i,i} + 2\mu u_{i,j} \bar{u}_{i,j}) \mathrm{d}\Omega = \int_\Omega \rho f_i \bar{u}_i \, \mathrm{d}\Omega. \tag{8}$$

Then the domain and velocity are discretized as

$$u_k = U_{k\lambda} N_\lambda \quad \text{and} \quad \bar{u}_i = \bar{U}_{i\alpha} N_\alpha \quad \text{on } \Omega_e, \tag{9}$$

where u_k and $\bar{u}_i$ are the velocity component and weighting function respectively and $U_{k\gamma}$ and $\bar{U}_{i\alpha}$ are the nodal values of u_k and $\bar{u}_i$ respectively.

The weak form is discretized as

$$\bar{U}_{i\alpha}(M_{i\alpha j\beta}\dot{U}_{j\beta} + C_{i\alpha j\beta}U_{j\beta} + N(u_i)_{i\alpha j\beta}) = \bar{U}_{i\alpha}F_{i\alpha}, \tag{10}$$

where

$$M_{i\alpha j\beta} = \int \rho N_\alpha N_\beta \delta_{ij} \, \mathrm{d}\Omega, \qquad C_{i\alpha j\beta} = \int (\lambda N_{\alpha,i} N_{\beta,j} + \mu N_{\alpha,j} N_{\beta,i} + \mu \delta_{ij} N_{\alpha,k} N_{\beta,k}) \, \mathrm{d}\Omega,$$

$$N(u_i)_{i\alpha j\beta} = \int \rho \delta_{ij} N_\alpha u_k u_{i,k} \, \mathrm{d}\Omega, \qquad F_{i\alpha} = \int N_\alpha f_i \, \mathrm{d}\Omega.$$

Then the finite element equation becomes

$$M_{i\alpha j\beta}\dot{U}_{j\beta} + C_{i\alpha j\beta}U_{j\beta} + N(u_i)_{i\alpha j\beta} = F_{i\alpha}. \tag{11}$$

To solve equation (11), the predictor–corrector method[20] is used. The algorithm of the predictor–corrector method is summarized as follows.

Predictor

$$\begin{aligned} \tilde{u}_{n+1} &= u_n + (1-\gamma)\Delta t a_n, \\ u^{(0)}_{n+1} &= \tilde{u}_{n+1}. \end{aligned} \tag{12}$$

Corrector

$$\text{From } l = 0 \text{ to } L\{(M_{i\alpha j\beta} + \gamma \Delta t C_{i\alpha j\beta}) U^{(l+1)}_{j\beta_{(n+1)}} = M_{i\alpha j\beta}\tilde{U}_{j\beta_{(n+1)}} + \gamma \Delta t (F_{i\alpha} - N(u^{(l)}_{i_{(n+1)}})_{i\alpha j\beta})\}, \tag{13}$$

$$\begin{aligned} u_{n+1} &= u^{(L+1)}_{n+1}, \\ a_{n+1} &= (u_{n+1} - \tilde{u}_{n+1})/\gamma \Delta t. \end{aligned} \tag{14}$$

Here u_n and a_n are the velocity and acceleration at the nth time iteration respectively, Δt is the time step, γ is a positive parameter which governs the stability and accuracy, and l and L are the iteration number and total number of corrector iterations respectively.

 © 1998 John Wiley & Sons, Ltd.

4. COMPUTATIONAL PROCEDURE

As shown in Figure 1, in the first stage of numerical analysis an initial grid is generated and values for the order of surface refinement and order of refinement expansion, material properties, boundary conditions and initial fractional volumes are input. Then the time step is increased and in each element the filling pattern is selected and the free surface is predicted by the filling pattern and smoothing techniques. In the next stage, by the refinement and mergence procedure an adaptive grid is generated, which also leads to the creation of the element domain for FEM analysis. Then by FEM analysis the velocity and pressure fields are obtained and the flow rate in each element is calculated. Subsequently the procedure of advection treatment is accomplished and the fractional volume in each element is obtained. These procedures are iterated until the current filling time reaches the total time.

4.1. Filling pattern in an element

In the Eulerian method, information on the shape of the free surface in an element is required to calculate the flow rate in the element. In the VOF method of Hirt and Nichols[10] the free surface is represented by horizontal and vertical line segments in square or rectangular cells. In Youngs' method[22] the line segment of the free surface is sloped in square cells. In the FLAIR method of Ashgriz and Poo[18] the line segments are drawn at the cell sides. In the reconstruction of the fluid volume by the code FIDAP[23] the filling shape is represented by rectangles or squares in the local element co-ordinate system for quadrilateral elements. In this study, to predict the free surface in a quadrilateral element, the filling pattern technique is proposed.

In the filling pattern technique the predicted free surface in a quadrilateral element is represented by a line segment with a slope. The predicted position of the free surface is calculated by using the fractional volume values under the assumption that the side wet ratios on each side or diagonal line to be partially wetted are constant. The side wet ratio is defined as

$$f_i^{\mathrm{b}} = l_i^{\mathrm{w}}/l_i, \tag{15}$$

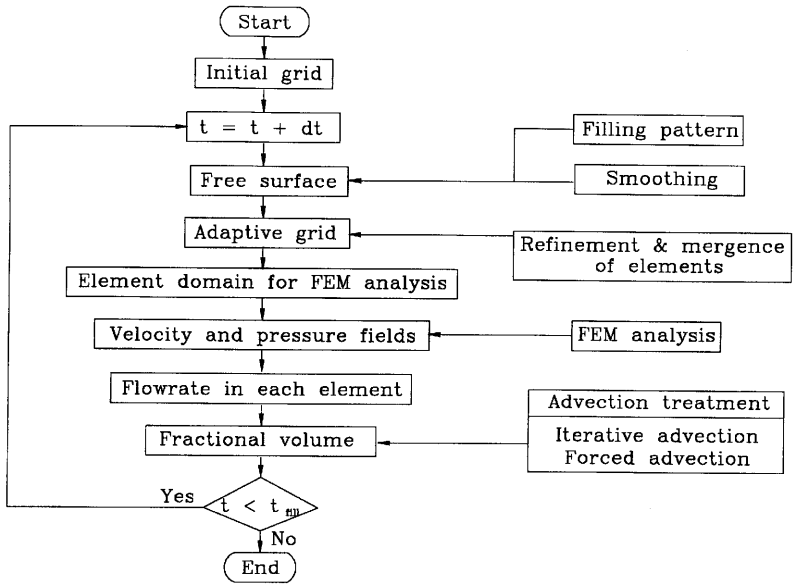

Figure 1. Flow chart of computational procedure.

© 1998 John Wiley & Sons, Ltd.

where f^{b}, l and l_i^{w} are the side wet ratio on side i, the total length of side i and the length of the wet region on side i respectively. The side wet ratio is used in calculating the side flow rate. The filling pattern technique can be viewed as being composed of two steps. First a filling pattern is determined among eight filling patterns. Then the predicted position of the free surface and the side wet ratio are calculated in each filling pattern. The filling pattern in an element depends only upon its filling state and the filling state of its neighbour elements, which are defined as elements sharing a common side, as shown in Figure 2. Then the predicted position of the free surface is calculated by the equations for geometrical shape considerations as shown in Figure 3. In Figure 3 the area of the hatched region in each filling pattern is equal to the volume of the fluid to be partially filled in an element. In all the filling patterns the side wet ratios of the sides to be partially wetted are categorized as follows:

$$
\begin{aligned}
&\text{case I,} && \alpha_{\mathrm{I}} = 0,\\
&\text{case II,} && \alpha_{\mathrm{II}} = 1,\\
&\text{case III,} && \vec{a}_2 \times \vec{a}_4\, \alpha_{\mathrm{III}}^2 - (\vec{a}_1 \times \vec{a}_2 - \vec{a}_1 \times \vec{a}_4)\alpha_{\mathrm{III}} + 2fV = 0,\\
&\text{case IV,} && \alpha_{\mathrm{IV}} = \sqrt{\left(\frac{2fV}{\vec{a}_1 \times \vec{a}_2}\right)},\\
&\text{case V,} && \alpha_{\mathrm{V}} = 1 - \sqrt{\left(\frac{2(f-1)V}{\vec{a}_4 \times \vec{a}_3}\right)},\\
&\text{case VI,} && \alpha_{\mathrm{VI}} = \sqrt{\left(\frac{2fV}{\vec{a}_1' \times \vec{a}_2' + \vec{a}_2' \times \vec{a}_3' + \vec{a}_3' \times \vec{a}_4' + \vec{a}_4' \times \vec{a}_1'}\right)},\\
&\text{case VII,} && \alpha_{\mathrm{VII}} = 1 - \sqrt{\left(\frac{2(1-f)V}{\vec{a}_1' \times \vec{a}_2' + \vec{a}_2' \times \vec{a}_3' + \vec{a}_3' \times \vec{a}_4' + \vec{a}_4' \times \vec{a}_1'}\right)},\\
&\text{case VIII,} && \alpha_{\mathrm{VIII}} = \frac{2fV}{(\vec{a}_1 - \vec{a}_3) \times \vec{a}_{\mathrm{s}}},
\end{aligned}
\tag{16}
$$

where f is the fractional volume and V the total volume of the element. Then, as shown in Figure 3, the side wet ratios for all sides can be expressed in the following categories:

$$
\begin{aligned}
&\text{case I,} && f_1^{\mathrm{b}} = \alpha_{\mathrm{I}}, \quad f_2^{\mathrm{b}} = \alpha_{\mathrm{I}}, \quad f_3^{\mathrm{b}} = \alpha_{\mathrm{I}}, \quad f_4^{\mathrm{b}} = \alpha_{\mathrm{I}},\\
&\text{case II,} && ,f_1^{\mathrm{b}} = \alpha_{\mathrm{II}}, \quad f_2^{\mathrm{b}} = \alpha_{\mathrm{II}}, \quad f_3^{\mathrm{b}} = \alpha_{\mathrm{II}}, \quad f_4^{\mathrm{b}} = \alpha_{\mathrm{II}},\\
&\text{case III,} && f_1^{\mathrm{b}} = 1, \quad f_2^{\mathrm{b}} = \alpha_{\mathrm{III}}, \quad f_3^{\mathrm{b}} = 0, \quad f_4^{\mathrm{b}} = \alpha_{\mathrm{III}},\\
&\text{case IV,} && f_1^{\mathrm{b}} = \alpha_{\mathrm{IV}}, \quad f_2^{\mathrm{b}} = \alpha_{\mathrm{IV}}, \quad f_3^{\mathrm{b}} = 0, \quad f_4^{\mathrm{b}} = 0\\
&\text{case V,} && f_1^{\mathrm{b}} = 1, \quad f_2^{\mathrm{b}} = 1, \quad f_3^{\mathrm{b}} = \alpha_{\mathrm{V}}, \quad f_4^{\mathrm{b}} = \alpha_{\mathrm{V}},\\
&\text{case VI,} && f_1^{\mathrm{b}} = 0, \quad f_2^{\mathrm{b}} = 0, \quad f_3^{\mathrm{b}} = 0, \quad f_4^{\mathrm{b}} = 0,\\
&\text{case VII,} && f_1^{\mathrm{b}} = 1, \quad f_2^{\mathrm{b}} = 1, \quad f_3^{\mathrm{b}} = 1, \quad f_4^{\mathrm{b}} = 1,\\
&\text{case VIII,} && f_1^{\mathrm{b}} = \alpha_{\mathrm{VIII}}, \quad f_2^{\mathrm{b}} = 0, \quad f_3^{\mathrm{b}} = \alpha_{\mathrm{VIII}}, \quad f_4^{\mathrm{b}} = 0.
\end{aligned}
\tag{17}
$$

 © 1998 John Wiley & Sons, Ltd.

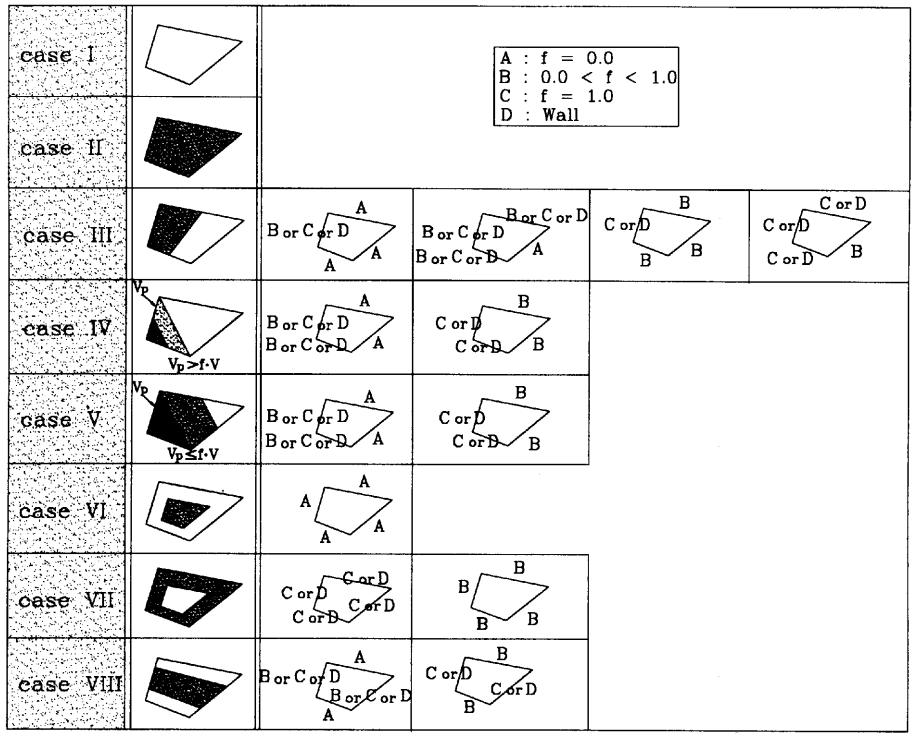

Figure 2. Filling patterns according to fractional volume and filling state in neighbour elements

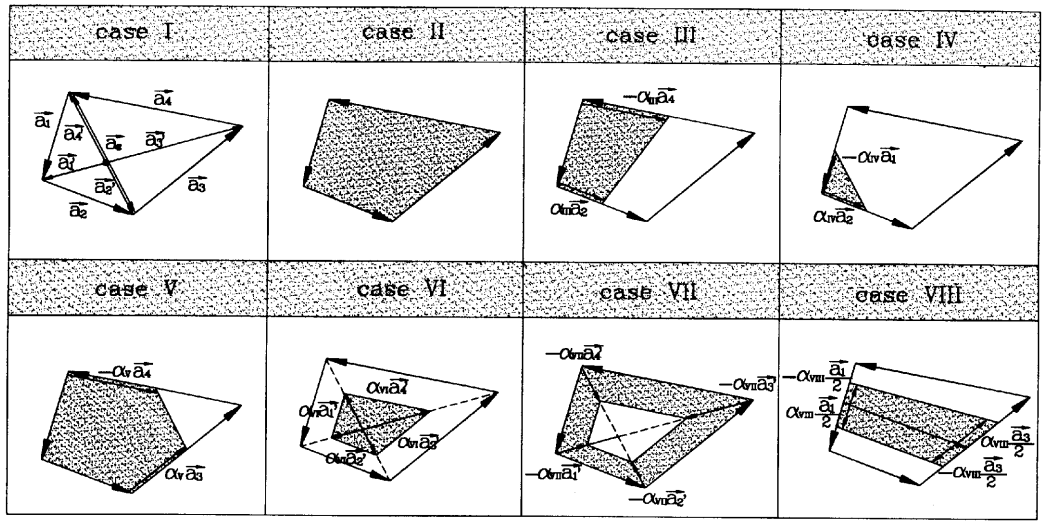

Figure 3. Geometrical description of filling patterns

© 1998 John Wiley & Sons, Ltd.

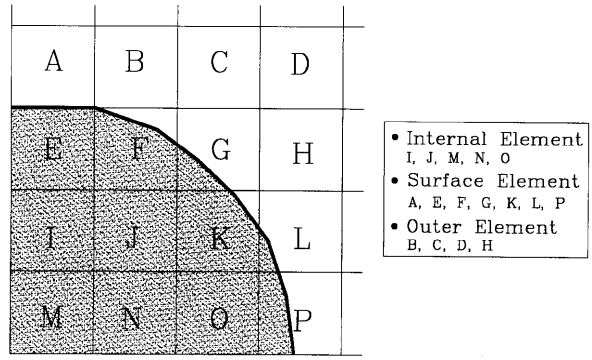

Figure 4. Definition of elements according to fractional volume and flow rate

4.2. *Flow rate in an element*

In the proposed numerical method, four-node quadrilateral elements for predicting the free surface and FEM analysis are used. The elements are sorted into three categories according to the fractional volume and the flow rate (Figure 4):

(i) internal element ($f=1$ and $\dot{Q}_{\text{in}}=0$)
(ii) surface element ($0 \leqslant f \leqslant 1$ and $\dot{Q}_{\text{in}} \neq 0$)
(iii) outer element ($f=0$ and $\dot{Q}_{\text{in}}=0$)

where f is the fractional volume and $\dot{Q}_{\text{in}}$ the flow rate of the element. The elements in the element domain are generated from the co-ordinates and connectivity of the internal and surface elements. The locations of the internal, surface and outer elements are inside, on the surface of and outside the fluid region respectively. The internal element is a filled element where the flow rate is zero. The surface element is a filled, partially filled or empty element where the flow rate is not zero, since the surface element includes the free surface. Therefore the element in which calculation of the flow rate is required is the surface element. The outer element is then an empty element in which the flow rate is zero.

The flow rate in a surface element is calculated by summation of the side flow rates (the flow rate of fluid across a side) on the four sides of the element. To calculate the side flow rate, the velocity field of the wetted side is required. It can be obtained by linear interpolation of the velocities at the vertex nodes. The side flow rate on a side is also obtained by summation of the outflow and inflow flow rates across the side. The side outflow and inflow rates are the flow rates to be calculated in the regions where the normal component velocities on the sides are negative and positive respectively. When using the donor–acceptor concept of Hirt *et al.*,[9] the side outflow and inflow rates must be calculated in an element and its neighbour element respectively. The absolute value of the side inflow rate in an element is equal to that of the side outflow rate in its neighbour element, with the signs being opposite. As shown in Figure 5, the side outflow rate, which is a negative value, is calculated as

$$\dot{q}^{\text{s}} = \int_{\partial\Omega_{\text{n}}} \vec{V} \cdot \vec{n} \, \mathrm{d}s, \tag{18}$$

where $\dot{q}^{\text{s}}$, $\vec{V}$ and $\vec{n}$ denote the side outflow rate, the velocity vector and the inward unit vector perpendicular to the side respectively, $\partial\Omega_{\text{n}}$ indicates the wetted region on the side of the element, where $\vec{V} \cdot \vec{n}$ is negative. In addition, for the sake of numerical stability, the specific advection that the fluid volume transfers from the partially filled element to the empty element is constrained. This

 © 1998 John Wiley & Sons, Ltd.

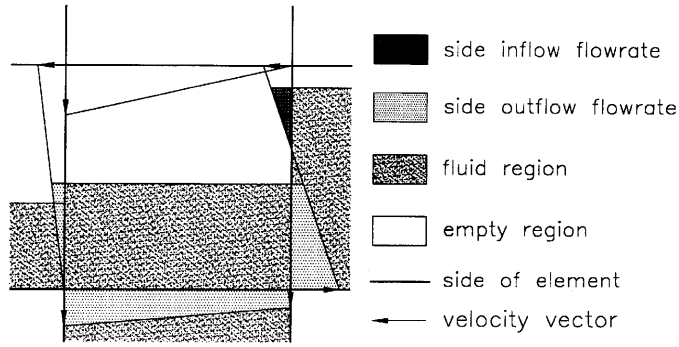

Figure 5. Definition of side inflow and outflow rates in an element

technique of constraining the specific advection of the fluid volume was proposed by Hirt *et al.*[9] Then the side flow rate $\dot{Q}^{\mathrm{s}}$ on a side is obtained from

$$\dot{Q}^{\mathrm{s}} = \dot{q}^{\mathrm{s}} - \dot{q}^{\mathrm{s^a}}, \tag{19}$$

where $\dot{q}^{\mathrm{s^a}}$ is the side outflow rate in a neighbour element. Finally, the flow rate $\dot{Q}_{\mathrm{in}}$ in an element can be expressed as

$$\dot{Q}_{\mathrm{in}} = \sum_{i=1}^{4} \dot{Q}_i^{\mathrm{s}}, \tag{20}$$

where $\dot{Q}_i^{\mathrm{s}}$ is the side flow rate through side i of the element.

4.3. Advection treatment

The advection of the fluid volume can be calculated from the assumption that the change in the fractional volume is proportional to the flow rate in the element during each small time step. With this assumption the fractional volume f_n can be expressed as

$$f_n = f_{n-1} + \Delta t^{\mathrm{f}} \dot{Q}_{\mathrm{in}} / V, \tag{21}$$

where f_n and f_{n-1} are the fractional volumes of an element time steps at n and $n+1$ respectively, Δt^f is the advection time step, V is the total volume of the element and $\dot{Q}_{\mathrm{in}}$ is the flow rate in the element. When using the prescribed advection time step, the fractional volume f_n calculated from (21) may become smaller than zero or larger than unity, such that advection treatment becomes necessary as shown in Figure 6. A simple advection treatment can be achieved by the flux-limiting method[9,23] as follows:

$$\Delta t^{\mathrm{f}} = |V_{\mathrm{o}} / \dot{Q}_{\mathrm{in}}|, \tag{22}$$

where

$$V_{\mathrm{o}} = \begin{cases} V f_{n-1} & \text{when } \dot{Q}_{\mathrm{in}} < 0, \\ V(f_{n-1} - 1) & \text{when } \dot{Q}_{\mathrm{in}} \geq 0. \end{cases}$$

Here V, f_{n-1} and $\dot{Q}_{\mathrm{in}}$ are the total volume of the element, the fractional volume at the previous time step and the flow rate in the element respectively. The advection time steps Δt^{f} are calculated in all the elements and the minimum value among the Δt^{f}s is selected. When the selected Δt^{f} is larger than the critical advection time step $\Delta t_{\mathrm{c}}^{\mathrm{f}}$ prescribed for numerical stability, Δt^{f} is replaced by $\Delta t_{\mathrm{c}}^{\mathrm{f}}$. This

© 1998 John Wiley & Sons, Ltd.

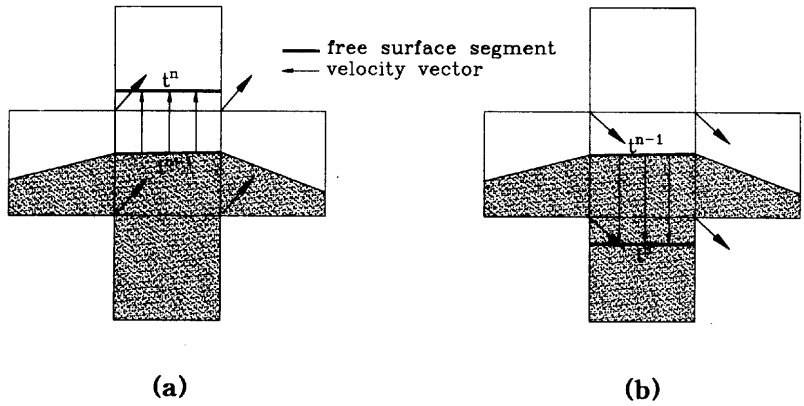

Figure 6. Schematic diagram of (a) over-filled and (b) over-emptied states in an element

prevents the transfer of more fluid volume than the acceptor element can receive and the transfer of more fluid than the donor element can give. This simple flux-limiting method is stable, but when the value of the calculated Δt^{f} is continuously small during the time iterations, the total number of iterations can become very large, leading to a long computation time.

In this study an iterative advection treatment is proposed. In this technique, if the calculated Δt^{f} is smaller than $\Delta t_{\mathrm{c}}^{\mathrm{f}}$, then only the advection treatment is repeated individually apart from the routine for FEM analysis. During the iterations for advection treatment the velocity and pressure values are fixed by assuming that the changes in velocity and pressure are very small since Δt^{f} is small. The merit of this technique is that the computation time for obtaining the velocity and pressure fields by FEM analysis can be reduced. The advection treatment iterations are carried out until the sum of the Δt^{f}s reaches $\Delta t_{\mathrm{c}}^{\mathrm{f}}$ or the fluid comes into contact with the pseudo wall side. As shown in Figure 7, the pseudo wall side is defined as the side including the two vertex nodes where the velocity is not calculated for the current time step. Therefore calculation of the side flow rate through the pseudo wall side is not possible and the iteration must be stopped.

For special cases where the changes in volume advection are very severe in a few elements such that the filling and emptying of the elements are continuously repeated, the computation time becomes very long. For such cases a forced advection treatment is proposed in this study for effective numerical analysis. As a similar study, in FIDAP[23] an advection adjustment method has been employed in which the factors representing the fractional area over which the fluid crosses the side are adjusted. In our forced advection treatment the fractional volumes are calculated in each element by using the prescribed $\Delta t_{\mathrm{c}}^{\mathrm{f}}$ and equation (21), and the fractional volumes of the elements that are larger than unity and smaller than zero are each adjusted to unity and zero respectively. Then, to compensate for the fluid volume, the fractional volumes of the neighbour elements are adjusted directly by utilizing weighting factors determined from the side flow rate calculated in the total region of the side in which the outflow exists, under the assumption that each side wet ratio is unity, as follows:

$$f^{\mathrm{A}_i'} = f^{\mathrm{A}_i} + \frac{V_{\mathrm{o}}}{V^{\mathrm{A}_i}} \frac{\dot{Q}_i^{\mathrm{A}}}{\sum_{i=1}^{4} \dot{Q}_i^{\mathrm{A}} w_i^{\mathrm{A}}} w_i^{\mathrm{A}}. \tag{23}$$

 © 1998 John Wiley & Sons, Ltd.

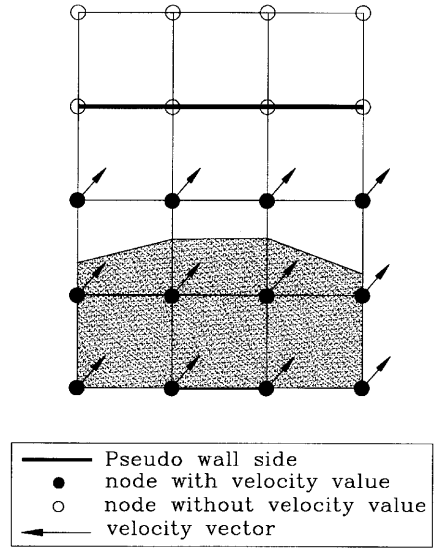

Figure 7. Schematic diagram of pseudo wall side

In (23),

$$V_o = \begin{cases} V_A f_A & \text{when } f_A < 0 \text{ (over-emptied case)}, \\ V_A(f_A - 1) & \text{when } f_A > 1 \text{ (over-filled case)}, \end{cases}$$

$$w_i^A = \begin{cases} 1 & \text{when } \dot{Q}_i^A < 0, \\ 0 & \text{when } \dot{Q}_i^A \geq 0, \end{cases}$$

where A is the over-emptied or over-filled element, A_i is the neighbour element of A, V^{A_i} is the volume of A_i, V^A is the volume of A, $\dot{Q}_i^A$ is the side flow rate calculated in the total region of side i of A under the assumption that the side wet ratio of side i is unity, f^A is the fractional volume of A, V_o is the compensation volume and w_i^A is the weighting factor for side i of A. The advection treatment is repeated until all over-filled and over-emptied elements are eliminated. If the element with the pseudo wall side is over-filled, than Δt_c^f is decreased and the forced advection procedure is repeated.

4.4. Adaptive grid

In general, when using a fixed grid, in order to obtain good numerical results, a large number of elements in the grid and the element domain for FEM analysis are required, since the initial elements must have a fine size. For a more efficient analysis, in this study an adaptive grid is generated by the refinement and mergence of the elements. An adaptive grid implies a grid where the internal and outer elements are coarse and the surface elements are relatively fine. An adaptive grid is regenerated at each time step when the location of the free surface is changed.

There are some noteworthy merits of the proposed technique using an adaptive grid. First of all, the accuracy of the numerical results is better than when using a fixed grid generated homogeneously with the same total number of elements, since the elements in the surface region for predicting the free surface and obtaining the velocity field are much finer than those in the inside region. Secondly, the required computation time and memory size are smaller than when using a fixed grid generated homogeneously with the same fine elements as those in the surface region of the adaptive grid.

© 1998 John Wiley & Sons, Ltd.

Thirdly, the size of elements can easily be changed by adjusting the order of surface refinement and the refinement expansion layer.

In order to generate an adaptive grid, first the surface elements, including the line segments of the free surface, are refined and the internal and outer elements that have been refined are merged. The procedure for generating an adaptive grid is summarized as follows.

Step 1. All elements are sorted into three categories: internal, surface and outer elements.
Step 2. The new surface elements at the current time step are refined until the refinement order reaches the prescribed surface refinement order.
Step 3. The new internal and outer elements that have been refined are merged.
Step 4. The procedure for refinement expansion is accomplished.

The procedure for refinement is accomplished by refining an element into four elements and the procedure for mergence is then followed by merging the four refined elements. In the process of refinement or mergence the difference in refinement order between an element and a neighbour element must be zero or unity, since for FEM analysis the element domain, where the total number of nodes on a side apart from vertex nodes cannot exceed one, is generated from a grid. Then, as shown in Figure 8, the procedures for refinement and mergence of an element are carried out if the following requirements are satisfied.

(i) Requirements for refinement of an element:
  (a) The category of an element is the surface element and the refinement order is smaller than the prescribed surface refinement order.
  (b) The category of an element is either the internal or the outer element and the element satisfies the condition

$$N - N^{\mathrm{a}} < -1, \tag{24}$$

  where N and N^{a} are the refinement orders of the element and a neighbour element respectively.

(ii) Requirements for mergence of an element:
  The category of an element is either the internal or outer element and the element satisfies the condition

$$N - N^{\mathrm{a}} > -1. \tag{25}$$

Then, in order to increase the stability of the numerical results, the procedure for refinement expansion is accomplished. In this procedure, layers of refined elements from the free surface are generated inside the fluid region. The total number of expansion layers is prescribed. The procedure for refinement expansion increases the number of elements and prevents the elements from being refined too drastically and excessively in the surface region of the element domain. The procedure for refinement in the surface region is accomplished stepwise from the zero refinement order to the prescribed refinement order. The procedure for mergence is carried out stepwise from the prescribed refinement order. The procedures for refinement and mergence are also accomplished during the procedure for advection treatment.

Then the element domain generated from an adaptive grid includes five-node elements. As shown in Figure 9, in order to treat the five-node elements, the following linear constraint equation[24] is used,

$$U^3_{\mathrm{mid}} = (U^1_{\mathrm{vertex}} + U^2_{\mathrm{vertex}})/2, \tag{26}$$

 © 1998 John Wiley & Sons, Ltd.

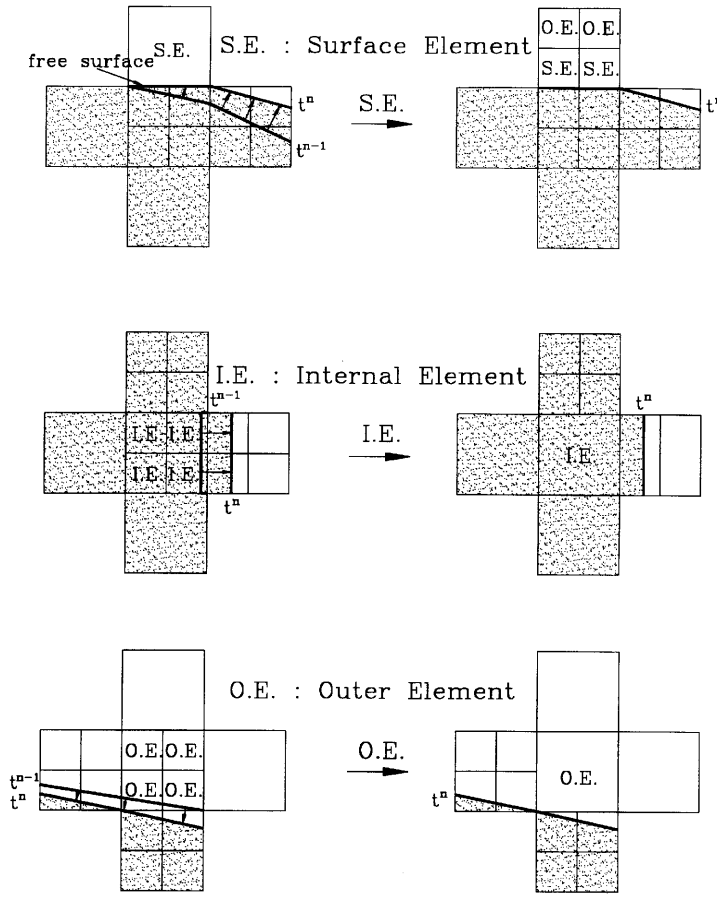

Figure 8. Procedures for refinement of a surface element and mergence of internal and outer elements

where U^3_{mid} is the velocity of the midside node and U^1_{vertex} and U^2_{vertex} are the velocities of vertex nodes 1 and 2 respectively. The arbitrary velocity inside element A becomes

$$\begin{aligned} u^{\text{A}} &= U^1_{\text{vertex}} N^1 + U^3_{\text{mid}} N^3 + U^5_{\text{vertex}} N^5 + U^4_{\text{vertex}} N^4 \\ &= U^1_{\text{vertex}} (N^1 + 0{\cdot}5N^3) + U^2_{\text{vertex}} 0{\cdot}5N^3 + U^5_{\text{vertex}} N^5 + U^4_{\text{vertex}} N^4, \end{aligned} \tag{27}$$

where U^1_{vertex}, U^2_{vertex}, U^3_{vertex}, U^4_{vertex} and U^5_{vertex} are the velocities of vertex nodes 1, 2, 3, 4 and 5 respectively and N^1, N^3, N^4 and N^5 are the shape functions of vertex nodes 1, 3, 4 and 5 respectively. From (27) the original connectivity [1, 3, 5, 4] of element A is replaced by [1, 2, 5, 4] and the shape functions [N^1, N^3, N^5, N^4] for calculating the stiffness matrix of element A are replaced by [$(N^1 + 0{\cdot}5N^3)$, $0{\cdot}5N^3$, N^5, N^4].

4.5. Smoothing of predicted free surface

The side wet ratios to be calculated with the selected filling pattern in each element are not continuous on the common side shared by two elements since they are calculated in each element

© 1998 John Wiley & Sons, Ltd.

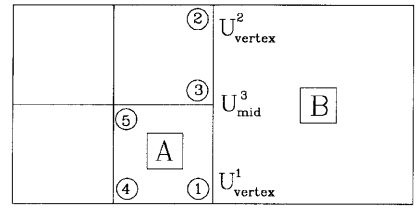

Figure 9. Configurations of a five-node element and its neighbour elements

independently. Also, in general, the predicted free surfaces can be expressed in a wavy form. Firstly, this is due to the fact that in an element the free surface is predicted by the filling pattern calculated only from the scalar functional volume value and the filling state of the neighbour elements. Secondly, for the sake of numerical stability, the specific advection of the fluid volume in a partially filled element into an empty element is constrained. Therefore a smoothing technique is developed in order to improve the non-smoothness of the predicted free surface. As shown in Figure 10, the smoothing procedure on the common side shared by two elements is summarized as follows.

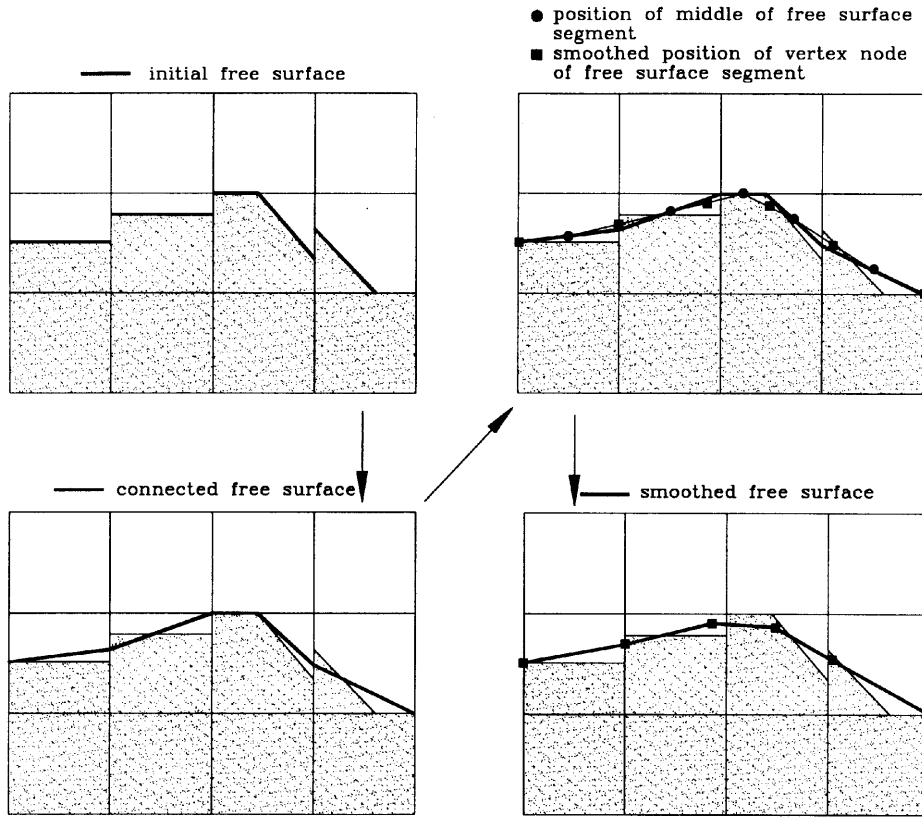

Figure 10. Procedure for smoothing of predicted free surface

 © 1998 John Wiley & Sons, Ltd.

Step 1. The segments of the free surface are connected by using the averaged values of the side wet ratio:

$$f_s^s = \begin{cases} (f_a^s + f_b^s)/2 & \text{when } 0 < f_a^s < 1 \text{ and } 0 < f_b^s < 1, \\ 1 & \text{when } f_a^s = 1 \text{ or } f_b^s = 1, \\ f_a^s & \text{when } f_b^s = 0, \\ f_b^s & \text{when } f_a^s = 0, \end{cases} \tag{28}$$

where 'a' and 'b' are the elements sharing a common side 's' and f_a^s and f_b^s are the side wet ratios of elements 'a' and 'b' respectively. In (28), if either f_a^s or f_b^s is unity, then f_s^s becomes unity in order to prevent the filled element from turning into a partially filled element. Also, if f_a^s or f_b^s is zero, then f_s^s becomes f_b^s or f_a^s respectively.

Step 2. The free surface is smoothed as follows:

$$X_{\text{smooth}}^a = (X_{\text{mid}}^p + X_{\text{mid}}^n)/2, \tag{29}$$

where X_{smooth}^a is the smoothed co-ordinate of node 'a' of the free surface segment and X_{mid}^p and X_{mid}^n are the co-ordinates of the midnodes of free surface segments 'p' and 'n' that share the common node 'a' respectively. Step 2 may be iterated to obtain a smoother free surface.

5. NUMERICAL ANALYSIS RESULTS OF PROBLEMS

Two examples, namely radial flow with a point source and the collapse of a dam, have been analysed using the adaptive element method. Each problem has been analysed using several grids to verify the efficiency of the adaptive element method. The numerical results are compared with theoretical solutions, experimental results and the numerical results of other cases.

5.1. Radial flow with a point source

In radial flow with a point source the fluid flows out from the point source at a constant flow rate. The constant values of density, viscosity and flow rate used in the numerical analysis are $\rho = 1$, $\mu = 1$ and $Q = 2\pi$ respectively and the critical advection time step Δt_c^f is 5×10^{-3} s. This is a one-dimensional flow problem with only the radial velocity component. However, for the two-dimensional analysis carried out in this study, as shown in Figure 11, the two-dimensional domain near a point source is used. When it is assumed that steady state flow occurs at each time step, the theoretical solution[17] in cylindrical co-ordinates is given by

$$U_r = 1/r, \qquad R = \sqrt{(2t)}, \qquad P = -2\mu/R^2 + \tfrac{1}{2}(R^{-2} - r^{-2}), \tag{30}$$

where U_r, r, R and P are the radial velocity, the radial distance from the point source, the position of the free surface and the pressure respectively.

In order to compare the numerical results for different cases, this problem has been analysed with a fixed grid (case I) and an adaptive grid (case II). The initial elements for cases I and II are shown in Figure 12. The total number of initial elements for case I is sixteen times that for case II. In order to test the effect of non-uniform elements, the initial grids are generated using elements of non-uniform shape. For case I the element configurations and predicted free surfaces at $t = 1{\cdot}5$, $2{\cdot}5$ and $3{\cdot}5$ s are shown in Figure 13. For case II the adaptive grids are shown in Figure 15. In Figure 14 the change in adaptive grid at each time step and the surface elements that are finer than other elements are shown. The element configurations and predicted free surfaces are shown in Figure 14. As seen in Figures 13 and 15, the element domains of case II are closer to the shape of the predicted free surface for each

© 1998 John Wiley & Sons, Ltd.

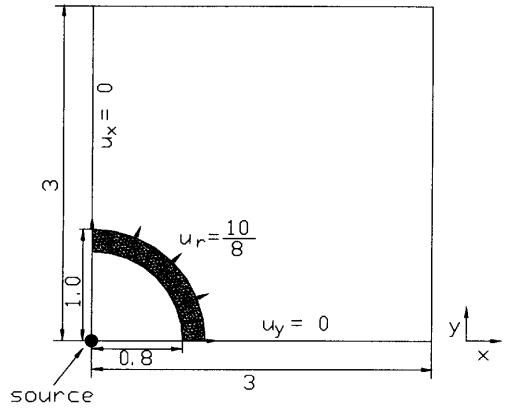

Figure 11. Schematic diagram of total and initial filled domains and boundary condition on wall

case than those of case I. Also, in case II the elements in the free surface region are finer than those in other regions. The free surface positions predicted in cases I and II are compared with the theoretical solutions in Figure 16 and Table I and the predicted pressures are compared with the theoretical solutions in Figure 17. In this problem, in order to compare more exactly the positions of predicted free surfaces, only step 1 of the smoothing procedure is carried out. The non- smoothness in Figures 16 and 17 occurs fundamentally from using the VOF method with a fixed grid, in contrast with the Lagrangian or ALE method in which the free surface can be predicted smoothly by using a movable grid. The free surface positions and predicted pressures in case II are closer to the theoretical solutions, since the elements in the surface region that are important for analysis are finer than those in case I. However, for both cases, deviation between the numerical results and theoretical solutions for pressure exists, since the numerical results are obtained from the transient state governing equation with a numerically small time step. This deviation can be decreased by using finer elements and smaller time steps. The average values of the total number of nodes and elements and the total computation time for cases I and II are given in Table II. It is seen that for case II a smaller memory size and a shorter computation time are required in comparison with case I. Thus the efficient use of elements is verified in the adaptive element method.

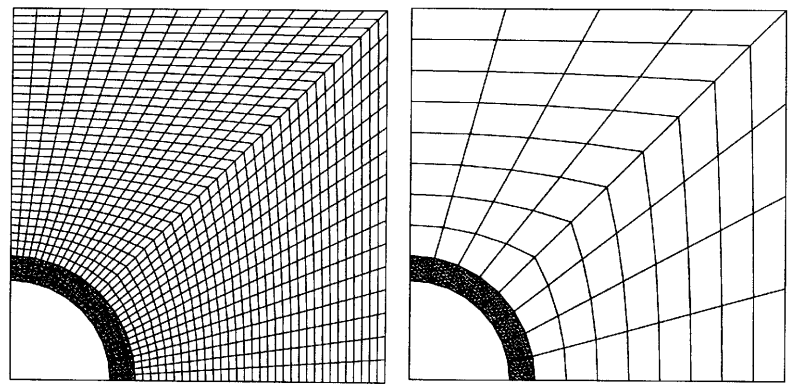

Figure 12. Initial grids in cases (a) I and (b) II

 © 1998 John Wiley & Sons, Ltd.

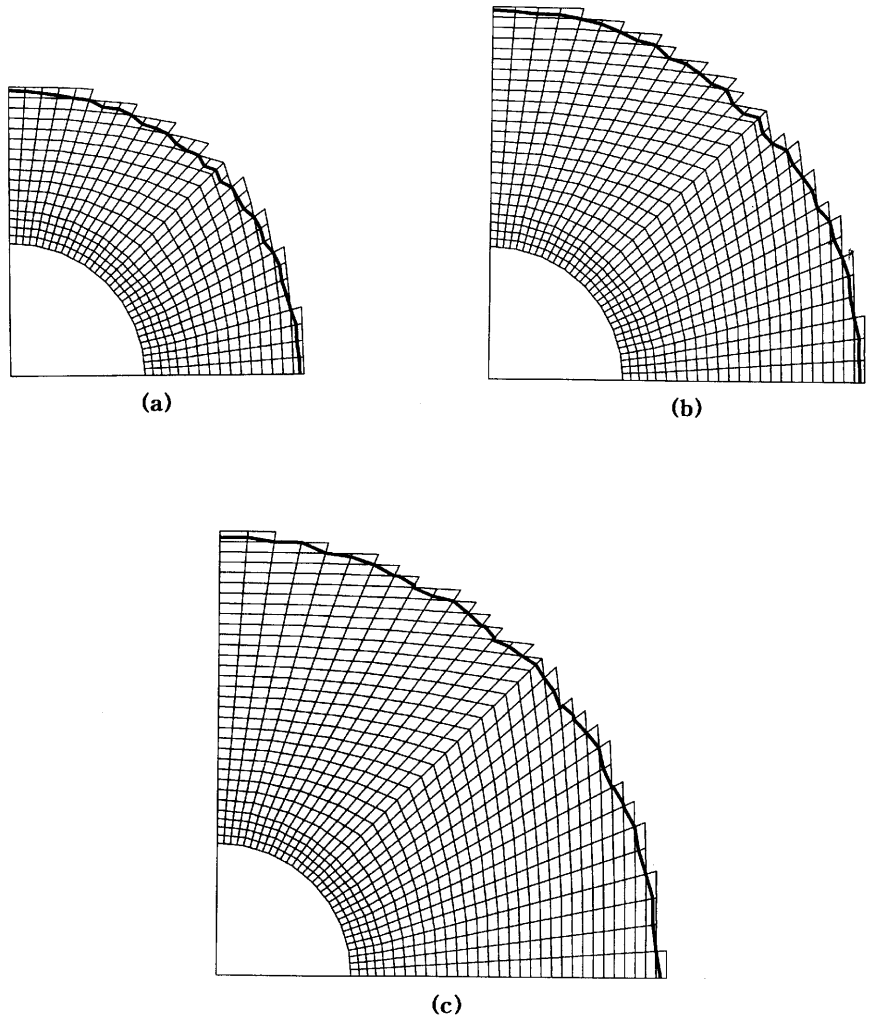

Figure 13. Predicted free surfaces and element configurations at (a) $t = 1{\cdot}5$, (b) 2·5 and (c) 3·5 s in case I

5.2. *Collapse of a dam*

The collapse of a dam is a typical problem used for verifying a new method for the analysis of transient fluid flow with a free surface. In this study, three grids for numerical analysis are used. Cases I and II use fixed grids, while case III uses an adaptive grid. The numerical results of all cases

Table I. Comparison of deviations between numerical results and theoretical solutions of free surface in both cases

	Fixed grid (case I)	Adaptive grid (case II)
Absolute maximum deviation	$3{\cdot}6 \times 10^{-2}$	$2{\cdot}5 \times 10^{-2}$
Absolute average deviation	$1{\cdot}0 \times 10^{-2}$	$6{\cdot}5 \times 10^{-3}$

© 1998 John Wiley & Sons, Ltd.

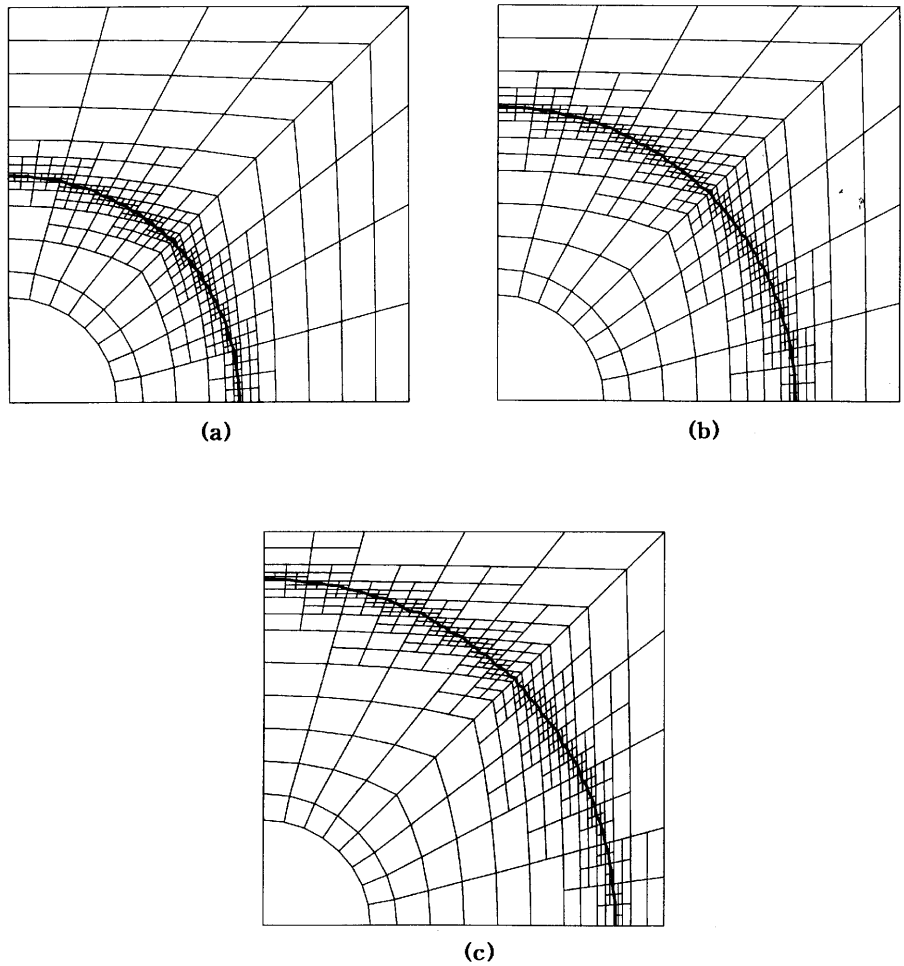

Figure 14. Predicted free surfaces and adaptive grids at (a) $t = 1{\cdot}5$, (b) 2·5 and (c) 3·5 s in case II

are compared with the experimental results of Martin and Moyce[25] and the predicted free surface positions of cases II and III are compared with those of case I, since neither experimental data nor theoretical solutions exist and the elements of case I are the finest amongst the three cases. In case II the total number of elements is only a quarter of that in case I, while in case III the total number of elements is only 1/64 of that in case I. As shown in Figure 18, the relative column height is $b/a = 2$.

Table II. Comparison of results obtained in both cases

	Fixed grid (case I)	Adaptive grid (case II)
Total number of nodal points	1152	388
Total number of elements	548	231
Total number of control volumes	606	326
Relative computational time	1	0·7

 © 1998 John Wiley & Sons, Ltd.

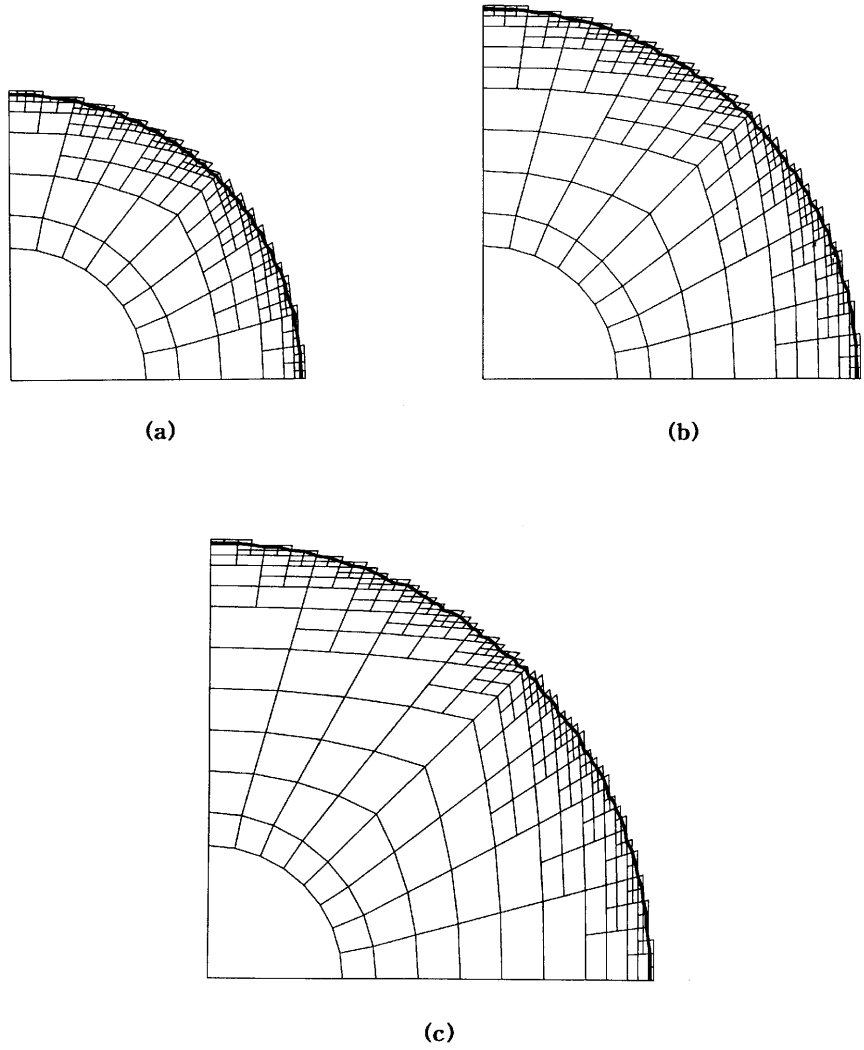

Figure 15. Predicted free surfaces and element configurations at (a) $t = 1{\cdot}5$, (b) 2·5 and (c) 3·5 s in case II

The density of water, its viscosity and the acceleration due to gravity are 1000 kg m^{-3}, 0·001 kg m^{-1} s^{-1} and 9·8 m s^{-2} respectively and the critical advection time step Δt_c is 2×10^{-4} s.

Figure 19 shows the initial element domains for cases I, II and III. With the dimensionless time and length defined as $T = t\sqrt{(2g/H)}$, for case I the element configurations and predicted free surfaces at $T = 1$, 2 and 2·9 are shown in Figure 20 and the velocity vectors in Figure 21. It is seen that the elements are fine and the velocities stable, since the elements in the initial grid are very fine. The predicted free surfaces are also seen to be very smooth and reasonable. Figures 22 and 23 show the element configurations, predicted free surfaces and velocity vectors for case II. In comparison with case I, the predicted free surfaces and velocities in regions near the wall are less smooth and more inaccurate. In case III the surface refinement order and refinement expansion layer are three and two respectively. The adaptive grids at each time step are shown in Figure 24. It is seen that the elements in the free surface region and refinement expansion layer are finer than in other regions. Figures 25

© 1998 John Wiley & Sons, Ltd.

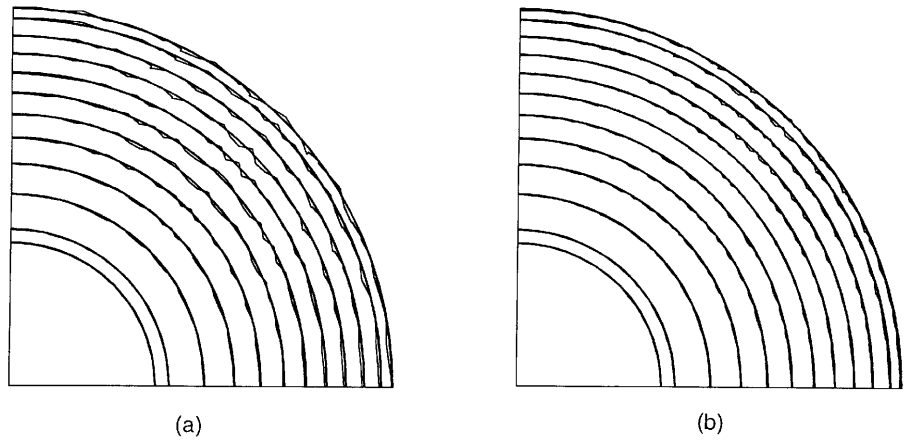

Figure 16. Predicted free surfaces (————) compared with theoretical solutions (————) in cases (a) I and (b) II

and 26 show the element configurations, free surfaces and velocity vectors for case III. It can be seen that the element domain where the elements in the surface region are fine is generated efficiently and the free surface and velocity field are predicted in a stable and effective manner. The positions of the predicted free surface along the bed are compared with Martin and Moyce's experimental results[25] in Figure 27. The predicted positions in cases I and III are very close to the experimental results. However, the numerical results for case II show some deviations from the experimental results, since the size of the elements is not sufficiently small to correctly predict the flow phenomena in the collapse of a dam. In Figure 28 the predicted free surface positions of cases II and III are compared with that of case I. The predicted free surface position of case III is closer to that of case I, since finer elements are used in the free surface region. The average values of the total number of nodes and elements and the total computation time in all cases are given in Table III. As can be seen, the largest

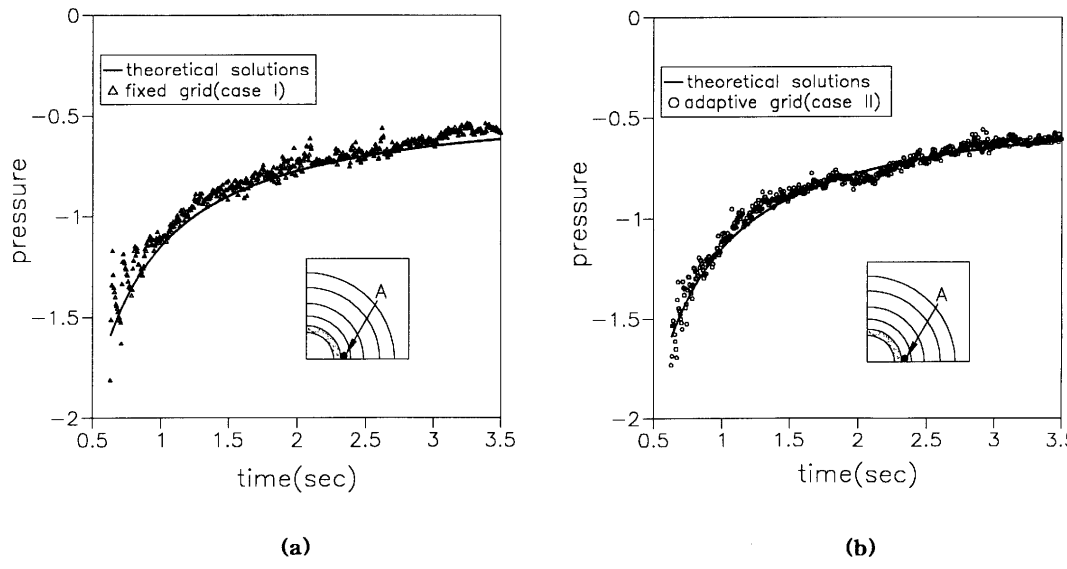

Figure 17. Predicted pressures versus time compared with theoretical solutions in cases (a) I and (b) II

 © 1998 John Wiley & Sons, Ltd.

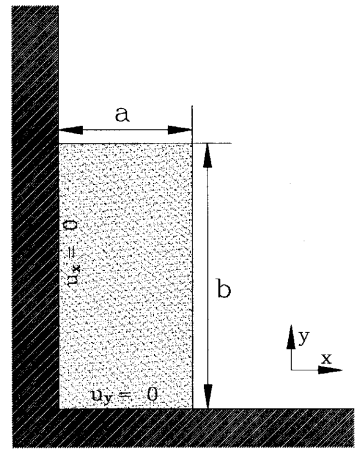

Figure 18. Schematic diagram of initial water column and wall boundary condition

Table III. Comparison of results obtained in all cases

	Fixed grid (case I)	Fixed grid (case II)	Adaptive grid (case III)
Total number of nodal points	2216	596	564
Total number of elements	2094	536	443
Total number of control volumes	12800	3200	970
Relative computational time	10·3	1	1·4

memory size and computation time were required for case I which had the largest number of elements in the initial grid. Case III was composed of the smallest number of elements, since the elements were used in an efficient way. However, case III required a longer computation time than case II by about 40 per cent because of the greater time consumed in the procedures of refinement and mergence of elements.

Finally, the numerical results of case III are much closer to those of case I and the experimental results compared with case II which employs more elements. The memory size required for case III is also smaller than that for cases I and II, while the total computation time is much shorter than that for case I and a little longer than that for case II. These numerical results have shown that an adaptive grid can be used efficiently for the analysis of transient fluid flow with a free surface.

CONCLUSIONS

The VOF method is adopted for the finite element analysis of transient fluid flow with a free surface. The proposed finite element analysis has two main features. First, an adaption technique for generating an adaptive grid is incorporated to capture a higher resolution of the free surface configuration. An adaptive grid in which the elements in the surface region are finer than those in other regions is created through procedures of refinement and mergence of elements. Secondly, the three techniques based on the VOF method are newly developed to increase the accuracy of the

© 1998 John Wiley & Sons, Ltd.

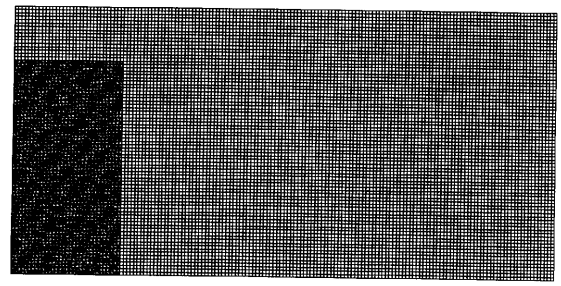

(a)

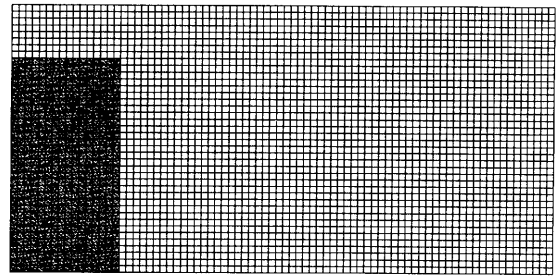

(b)

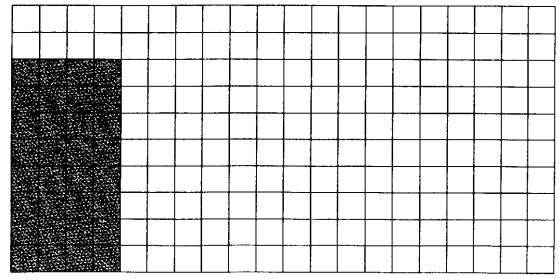

(c)

Figure 19. Initial grids and filled regions in cases (a) I, (b) II and (c) III

© 1998 John Wiley & Sons, Ltd.

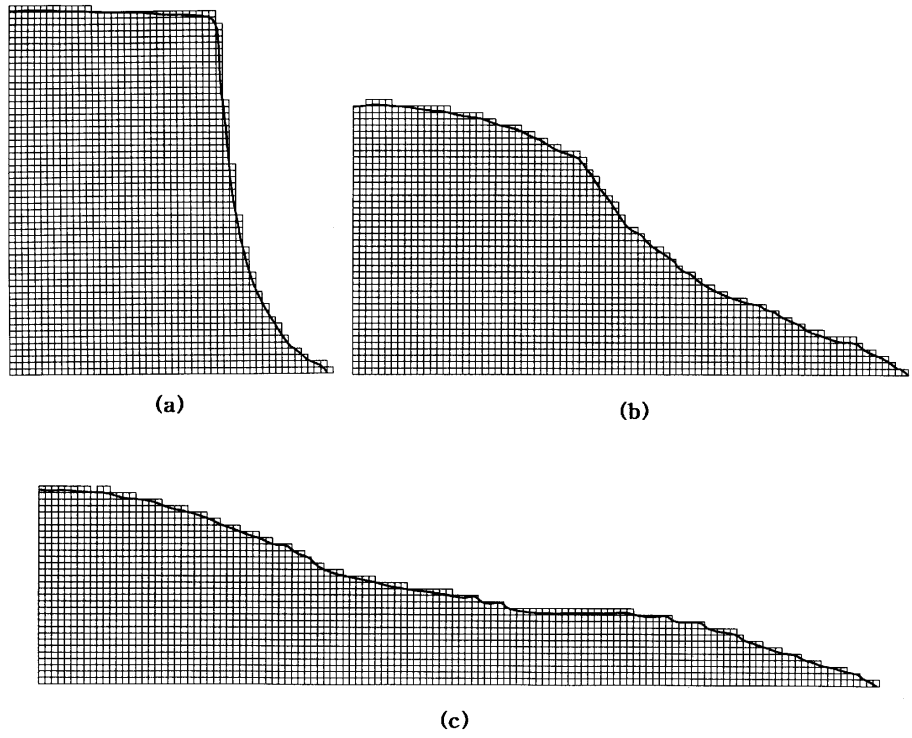

Figure 20. Predicted free surfaces and element configurations at $T=$ (a) 1, (b) 2 and (c) 2·9 in case I

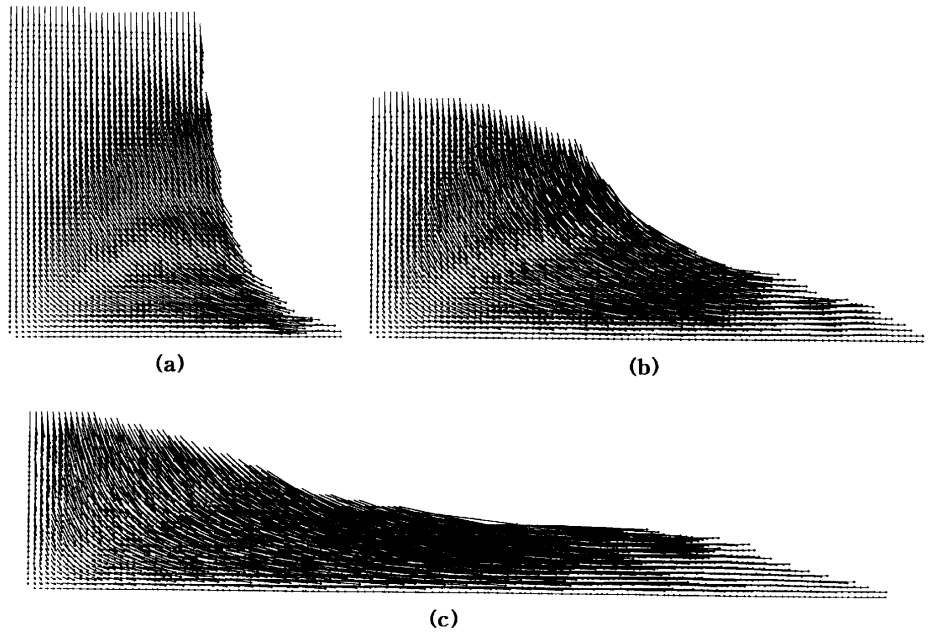

Figure 21. Velocity fields at (a) $T=$ (a) 1, (b) 2 and (c) 2·9 in case I

© 1998 John Wiley & Sons, Ltd.

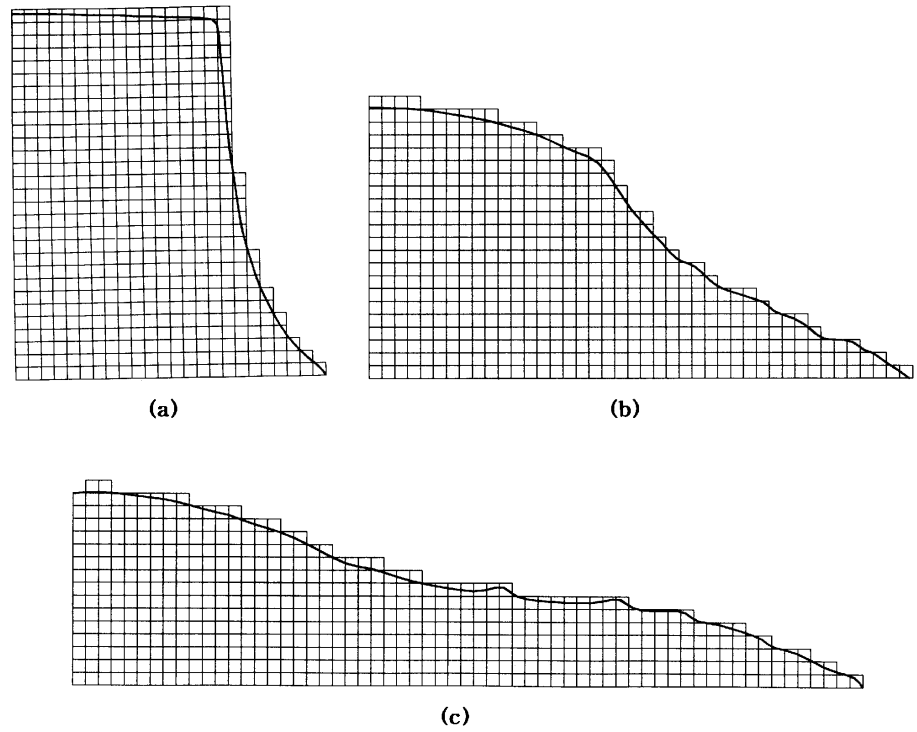

Figure 22. Predicted free surfaces and element configurations at $T=$(a) 1, (b) 2 and (c) 2·9 in case II

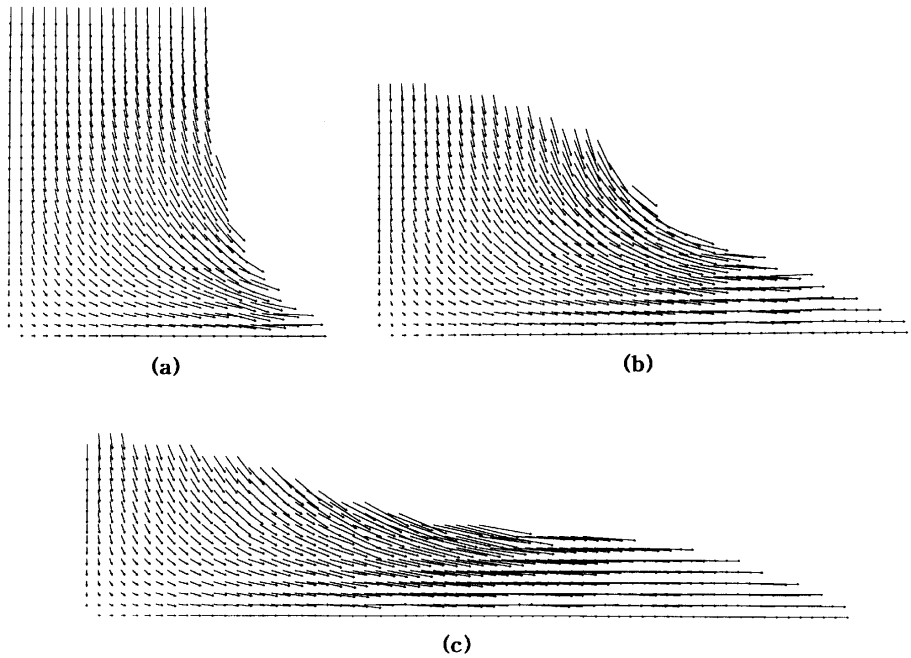

Figure 23. Velocity fields at $T=$(a) 1, (b) 2 and (c) 2·9 in case II

 © 1998 John Wiley & Sons, Ltd.

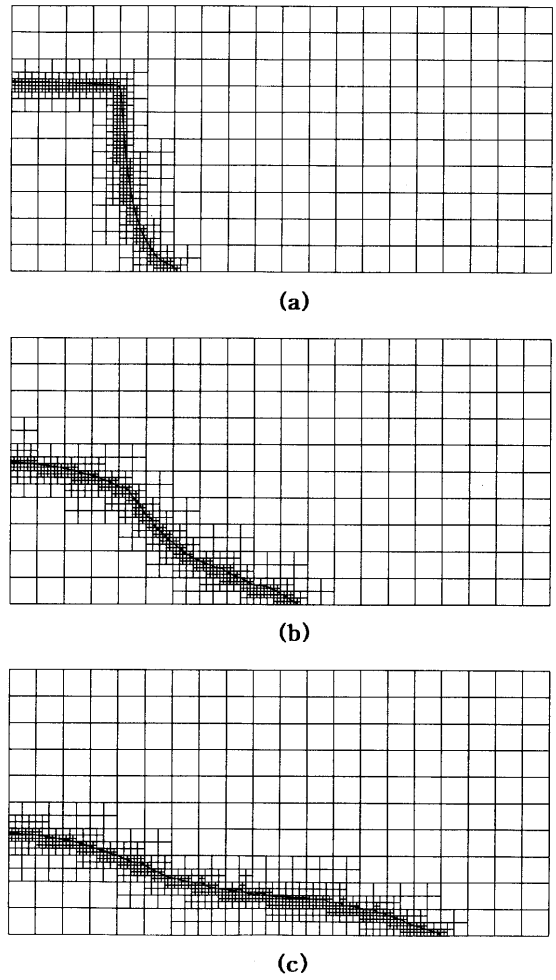

Figure 24. Predicted free surfaces and adaptive grids at $T=$ (a) 1, (b) 2 and (c) 2·9 in case III

© 1998 John Wiley & Sons, Ltd.

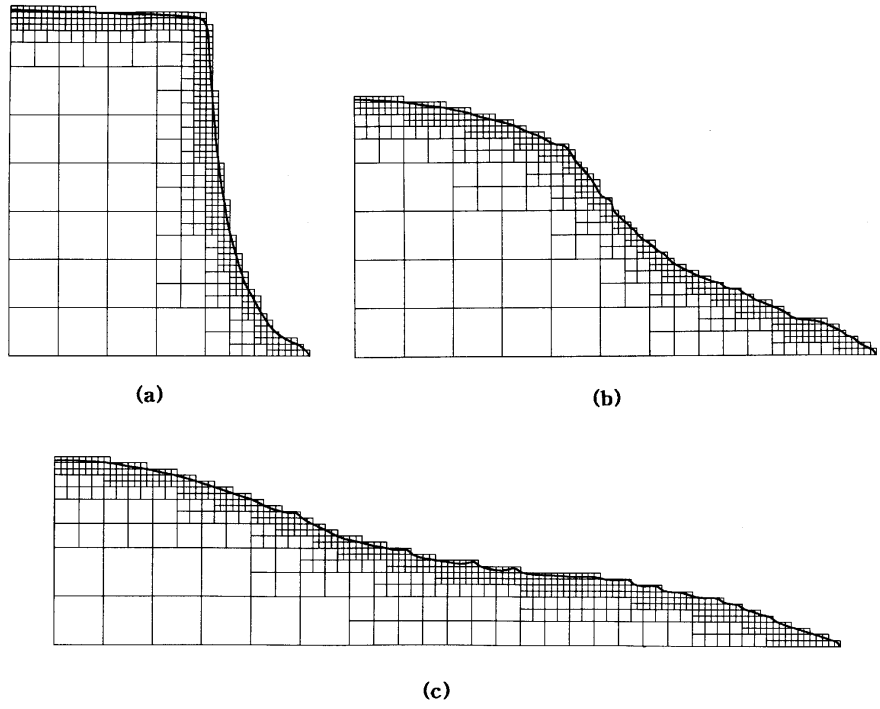

Figure 25. Predicted free surfaces and element configurations at $T=$(a) 1, (b) 2 and (c) 2·9 in case III

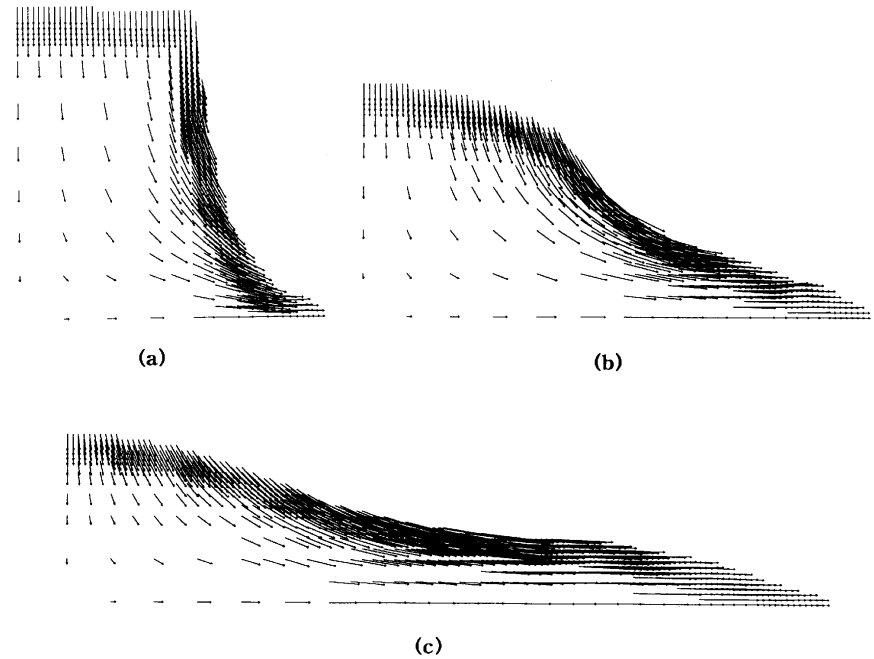

Figure 26. Velocity fields at $T=$(a) 1, (b) 2 and (c) 2·9 in case III

 © 1998 John Wiley & Sons, Ltd.

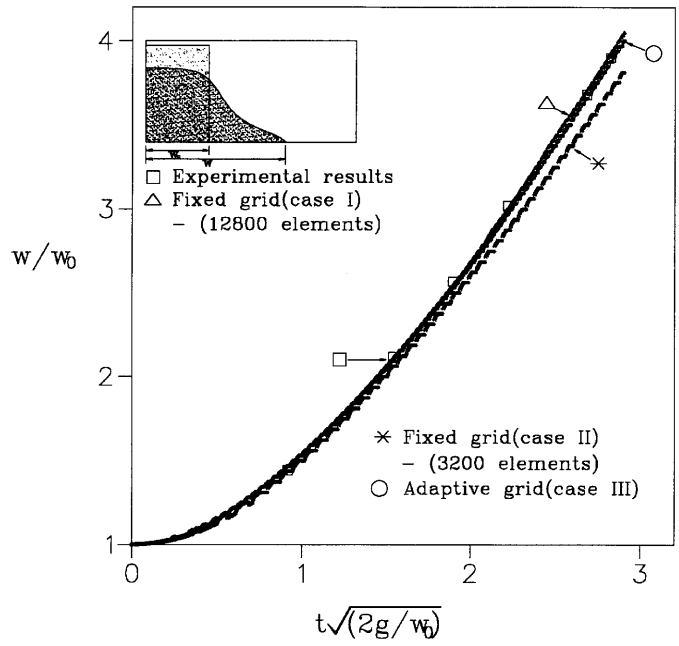

Figure 27. Predicted front position variation versus time compared with experimental results of Martin and Moyce[25]

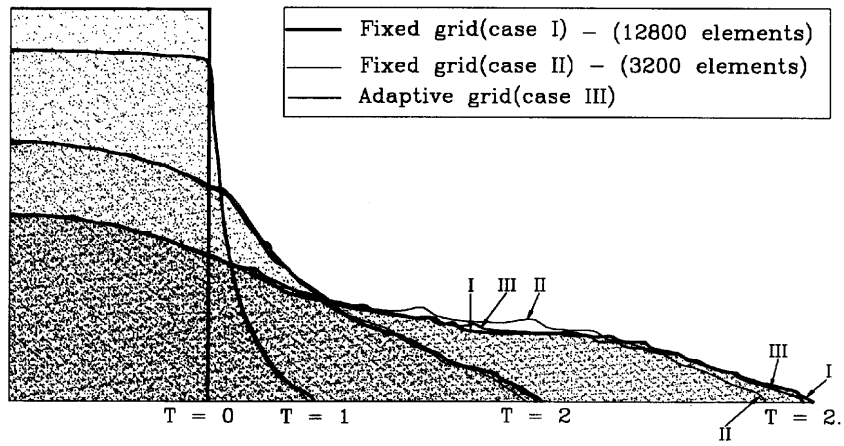

Figure 28. Comparison of predicted free surfaces in all cases

analysis. The first approach is the filling pattern technique to predict the free surface by considering the geometric shape of each quadrilateral element. The second approach is the advection treatment technique to calculate the fluid advection iteratively and forcedly. The third approach is the smoothing technique to improve the non-smoothness of the predicted free surface. In particular, for complex problems the accuracy of the numerical results can be improved by the additional refinement of elements inside the specific domain. Radial flow with a point source and the collapse of a dam

© 1998 John Wiley & Sons, Ltd.

have been analysed. The numerical results agree well with the theoretical solutions and experimental results. The numerical analyses were carried out for several cases using different grids. Through comparisons of the numerical results of several cases, the efficiency of the proposed method is checked and it can be further applied to problems of transient fluid flow with a free surface.

REFERENCES

1. B. Ramaswamy and M. Kawahara, 'Lagrangian finite element analysis applied to viscous free surface fluid flow', *Int. j. numer. meth. fluids*, **7**, 953–984 (1987).
2. F. Muttin, T. Coupez, M. Bellet and J. L. Chenot, 'Lagrangian finite-element analysis of time-dependent viscous free-surface flow using an automatic remeshing technique: Application to metal casting flow', *Int. j. numer. meth. engng.*, **36**, 2001–2015 (1993).
3. C. W. Hirt, A. A. Amsden and J. L. Cook, 'An arbitrary Lagrangian–Eulerian computing method for all flow speeds', *J. Comput. Phys.*, **14**, 227–253 (1974).
4. R. K.-C. Surname, 'A generalized arbitrary Lagrangian–Eulerian method for incompressible flows with sharp interfaces', *J. Comput. Phys.*, **58**, 311–331 (1975).
5. W. K. Liu, H. Chang, J. S. Chen and T. Belytschko, 'Arbitrary Lagrangian–Eulerian Petrov–Galerkin finite elements for nonlinear continua', *Comput. Meth. Appl. Mech. Engng.*, **68**, 259–310 (1988).
6. F. H. Harlow and J. E. Welch, 'Numerical calculation of time-dependent viscous incompressible flow of fluid with free surface', *Phys. Fluids*, **8**, 2182–2189 (1965).
7. A. A. Amsden and E. H. Harlow, 'The SMAC method: a numerical technique for calculating incompressible fluid flows', *Los Alamos Scientific Laboratory Rep. LA-4370*, University of California, 1970.
8. T. Nakayama and M. Mory, 'An Eulerian finite element method for time dependent free surface problems in hydrodynamics', *Int. j. numer. meth. fluids*, **22**, 175–194 (1996).
9. C. W. Hirt, B. D. Nichols and N. C. Romero, 'SOLA-VOF: a solution algorithm for transient fluid flows', *Los Alamos Scientific Laboratory Rep. LA-5852*, University of California, 1975.
10. C. W. Hirt and B. D. Nichols, 'Volume of fluid (VOF) method for the dynamics of free boundaries', *J. Comput. Phys.*, **39**, 201–225 (1981).
11. E. Thompson, 'Use of pseudo-concentrations to follow creeping viscous flows during transient analysis', *Int. j. numer. meth. fluids*, **6**, 749–761 (1986).
12. G. Dhatt, D. M. Gao and A. Ben Cheikh, 'A finite element simulation of metal flow in moulds', *Int. j. numer. meth. engng.*, **30**, 821–831 (1990).
13. K. S. Chan, K. Pericleous and M. Cross, 'Numerical simulation of flows encountered during mold-filling', *Appl. Math. Model.*, **15**, 624–631 (1991).
14. A. S. Usmani, J. T. Cross and R. W. Lewis, 'A finite element model for the simulations of mould filling in metal casting and the associated heat transfer', *Int. j. numer. meth. engng.*, **35**, 787–806 (1992).
15. E. Broyer, C. Gutfinger and Z. Tadmor, 'A theoretical model for the cavity filling process in injection molding', *Trans. Soc. Rheol.*, **19**, 423–444 (1975).
16. K. K. Wang, *et al.*, 'Computer-aided design and fabrication of molding and computer control of injection molding', *Prog. Rep. 11*, Cornell University, Ithaca, NY, 1986.
17. S. P. Wang and K. K. Wang, 'A net inflow method for incompressible viscous flow with moving free surface', *Int. j. numer. meth. fluids*, **18**, 669–694 (1994).
18. N. Ashgriz and J. Y. Poo, 'FLAIR: flux line-segment model for advection and interface reconstruction', *J. Comput. Phys.*, **93**, 449–468 (1991).
19. F. Mashayek and N. Ashgriz, 'A hybrid finite-element–volume-of-fluid method for simulation of free surface flows and interfaces', *Int. j. numer. meth. fluids*, **20**, 1363–1380 (1995).
20. T. J. R. Hughes, W. K. Liu and A. Brooks, 'Finite element analysis of incompressible viscous flows by the penalty function formulation', *J. Comput. Phys.*, **30**, 1–60 (1979).
21. N. Kikuchi, *Finite Element Methods in Mechanics*, Cambridge University Press, New York, 1986.
22. D. L. Youngs, 'Time-dependent multi-material flow with large fluid distortion', *Numer. Meth. Fluid Dyn.*, **00**, 273–285 (1982).
23. *FIDAP 7.5 Update Manual*, 1995.
24. K. J. Bathe, *Finite Element Procedure in Engineering Analysis*, Prentice-Hall, Englewood Cliffs, NJ, 1982.
25. J. C. Martin and W. J. Moyce, 'An experimental study of the collapse of liquid columns on a rigid horizontal plane', *Philos. Trans. A*, **244**, 312–324 (1952).

 © 1998 John Wiley & Sons, Ltd.